

Forest floor fluxes drive differences in the carbon balance of contrasting boreal forest stands

Jinshu Chi^{a,*}, Peng Zhao^a, Anne Klosterhalfen^a, Georg Jocher^b, Natascha Kljun^c, Mats B. Nilsson^a, Matthias Peichl^a

^a Department of Forest Ecology and Management, Swedish University of Agricultural Sciences, Umeå, Sweden

^b Department of Matter and Energy Fluxes, Global Change Research Institute, Czech Academy of Sciences, Brno, Czech Republic

^c Centre for Environmental and Climate Science, Lund University, Lund, Sweden

ARTICLE INFO

Keywords:

Forest floor
Understory vegetation
Eddy covariance
CO₂ fluxes
Boreal forest

ABSTRACT

The forest floor provides an important interface of soil-atmosphere CO₂ exchanges but their controls and contributions to the ecosystem-scale carbon budget are uncertain due to measurement limitations. In this study, we deployed eddy covariance systems below- and above-canopy to measure the spatially integrated net forest floor CO₂ exchange (NFFE) and the entire net ecosystem CO₂ exchange (NEE) at two mature contrasting stands located in close vicinity in boreal Sweden. We first developed an improved cospectra model to correct below-canopy flux data. Our empirical below-canopy cospectra models revealed a greater contribution of large- and small-scale eddies in the trunk space compared to their distribution in the above-canopy turbulence cospectra. We found that applying the above-canopy cospectra model did not affect the below-canopy annual CO₂ fluxes at the sparse pine forest but significantly underestimated fluxes at the dense mixed spruce-pine stand. At the mixed spruce-pine stand, forest floor respiration (R_{ff}) was higher and photosynthesis (GPP_{ff}) was lower, leading to a 1.4 times stronger net CO₂ source compared to the pine stand. We further found that drought enhanced R_{ff} more than GPP_{ff} , leading to increased NFFE. Averaged across the six site-years, forest floor fluxes contributed 82% to ecosystem-scale respiration (R_{eco}) and 12% to gross primary production (GPP). Since the annual GPP was similar between both stands, the considerable difference in their annual NEE was due to contrasting R_{eco} , the latter being primarily driven by the variations in NFFE. This implies that NFFE acted as the driver for the differences in NEE between these two contrasting stands. This study therefore highlights the important role of forest floor CO₂ fluxes in regulating the boreal forest carbon balance. It further calls for extended efforts in acquiring high spatio-temporal resolution data of forest floor fluxes to improve predictions of global change impacts on the forest carbon cycle.

1. Introduction

Boreal forests occupy ~30% of the global forest area and significantly affect the global carbon (C) cycle and climate (Bonan, 2008; Pan et al., 2011). The forest C balance however strongly depends on the exchanges of carbon dioxide (CO₂) with the atmosphere across different vertical canopy layers (Fatichi et al., 2019; Katul and Albertson, 1999; Tarvainen et al., 2020). These include tree canopy foliage, woody elements, and the various CO₂ sources and sinks existing at the forest floor interface (soil, tree roots, woody debris, and understory vegetation). The photosynthesis of understory vegetation (GPP_{ff}) and the forest floor respiration (R_{ff}) represent major pathways of assimilating and releasing

CO₂ between the forest floor and the atmosphere, respectively (e.g., Misson et al., 2007; Paul-Limoges et al., 2017). Given that various components contribute to the forest floor CO₂ exchanges such as heterotrophic respiration from the mineralization of organic matter, tree root respiration as well as understory vegetation autotrophic respiration and photosynthesis (Ryhti et al., 2021), the CO₂ fluxes may have large spatial variabilities over the heterogeneous forest floor, depending on site characteristics, such as understory vegetation species and distribution, soil properties, overstory canopy openness and density, below-ground allocation of photosynthates and root biomass distribution (Goulden and Crill, 1997; Kulmala et al., 2019; Palmroth et al., 2019). Thus, the forest floor CO₂ exchange is a complex composite of

* Corresponding author.

E-mail address: jinshu.chi@slu.se (J. Chi).

<https://doi.org/10.1016/j.agrformet.2021.108454>

Received 15 December 2020; Received in revised form 23 April 2021; Accepted 26 April 2021

Available online 21 May 2021

0168-1923/© 2021 The Author(s). Published by Elsevier B.V. This is an open access article under the CC BY license (<http://creativecommons.org/licenses/by/4.0/>).

various processes and in-depth knowledge of its dynamics and controls is required for better understanding its role in the boreal forest C cycle.

To date, forest floor CO₂ fluxes in boreal forests have been measured mainly using the chamber technique (e.g., Bergeron et al., 2009; Gaumont-Guay et al., 2014; Goulden and Crill, 1997; Hasselquist et al., 2012; Kolari et al., 2006; Morén and Lindroth, 2000; Palmroth et al., 2019; Swanson and Flanagan, 2001). However, chamber measurements provide flux data from plot-scale, which may not result in a spatially well-integrated CO₂ flux estimate over the heterogeneous forest floor. Manual chamber measurements are also commonly carried out in coarse weekly to biweekly intervals and thus further lack sufficient temporal resolution. A comprehensive understanding of the magnitude, variations, and controls of the forest floor C budget however requires high-temporal resolution (e.g., using automated chamber systems) and long-term (e.g., more than five years) measurements (Gaumont-Guay et al., 2014; Kulmala et al., 2019; Teramoto et al., 2017). In addition, in the boreal region, chamber measurements are commonly conducted only during the growing season (e.g., Bergeron et al., 2009; Hasselquist et al., 2012; Palmroth et al., 2019), whereas information on forest floor CO₂ flux dynamics during the long-lasting (~6+ months) and mostly snow-covered non-growing season is limited.

Alternatively, the eddy covariance (EC) method provides integrated flux estimates from subcanopy to ecosystem scales and from high-temporal (i.e., half-hourly) to annual scales (Baldocchi, 2003; Baldocchi and Meyers, 1991). To date, however, only a limited number of studies have estimated forest floor CO₂ fluxes using the EC technique. Furthermore, these studies have been conducted in mostly temperate and high-latitude regions (e.g., Black et al., 1996; Constantin et al., 1999; Falk et al., 2005; Jocher et al., 2017; Kulmala et al., 2019; Paul-Limoges et al., 2017). The limited number of below-canopy EC studies is primarily due to the challenges and concerns about potential violations of underlying assumptions when applying the EC method in the trunk space. Due to multiple concurrent mechanisms such as wind inflection by tree trunks and aerodynamic drag on the foliage, turbulence in the trunk space is more complex and thus hardly ever in accordance with the universal theories describing the above-canopy and surface-layer turbulence characteristics (Finnigan, 2000; Launiainen et al., 2005; Vickers and Thomas, 2014). Ignoring the fundamentals of turbulent transport processes in trunk space may lead to biased EC measurements. Nevertheless, below-canopy EC studies have commonly applied the traditional above-canopy cospectra model to correct the below-canopy EC measurements, mostly due to the lack of existing below-canopy models (Launiainen et al., 2005). However, the expected discrepancies observed in previous studies (e.g., Brunet, 2020; Finnigan, 2000) in above- and below-canopy turbulence suggest the need for a distinct below-canopy cospectra model to ensure accurate EC measurements in the forest trunk space.

Due to the various limitations in both chamber and below-canopy EC data, large uncertainties still exist in the seasonal and inter-annual variabilities of forest floor fluxes and their contribution to ecosystem C budgets. In addition, accurate measurements are also the pre-requisite for investigating the response of forest floor fluxes to external perturbations. The boreal region is particularly sensitive to rapid climate change with more pronounced warming during the non-growing season than the growing season in northern Sweden (Teutschbein et al., 2015). While studies have suggested a future increase in forest productivity in boreal forests (Henttonen et al., 2017; Poudel et al., 2011), changing environmental conditions (e.g., extensive heat and drought) may also considerably accelerate the forest floor CO₂ emissions (Jarosz et al., 2008; Kotani et al., 2019; Palmroth et al., 2005) thus counterbalancing the enhanced C uptake by trees. Extreme weather events, such as drought, have significantly affected the carbon and energy budgets of the European forests (Bastos et al., 2020; Ciais et al., 2005; Graf et al., 2020; Lindroth et al., 2020) and boreal forests worldwide (e.g., Kljun et al., 2007; Ma et al., 2012; Welp et al., 2007). However, the separate responses of the tree canopy and forest floor CO₂ exchanges to the warm

and dry conditions remain elusive. For example, drought can reduce root respiration (Griffis et al., 2004; Reichstein et al., 2007), increase heterotrophic respiration (Lindroth et al., 2020), and inhibit understory vegetation photosynthesis (Kotani et al., 2019). A detailed understanding of the CO₂ fluxes from the various forest ecosystem components is essential to investigate global change impacts on boreal forest ecosystems and improve model simulations.

In this study, we applied the EC technique to estimate the CO₂ exchanges of the forest floors covered by dwarf shrubs and a ground layer of mosses in two adjacent (~10 km) but contrasting boreal forests, i.e., a pine stand with open trunk space and a mixed spruce-pine stand with dense trunk space in boreal Sweden from 2016 to 2019. The specific objectives were to 1) develop a below-canopy cospectra model to correct EC data collected in the trunk space; 2) quantify the magnitudes and seasonal patterns of forest floor CO₂ fluxes; 3) estimate their contribution to the ecosystem-scale C budgets; and 4) investigate their responses to environmental factors across two contrasting boreal forest stands.

2. Methods

2.1. Site description

The study was conducted at two forest stands near Vindeln, Västerbotten, Sweden. The Rosinedalsheden (ROS) site (64°10'N, 19°45'E, 145 m a.s.l.) is a ~100-year-old naturally regenerated homogenous pine (*Pinus sylvestris*) stand that grows on sandy soils (Lim et al., 2015). The mean tree height at ROS increased from 18.5 m to 19.1 m during 2016-2019. Located 10 km north of ROS is the Svartberget (SVB) experimental forest (64°15'N, 19°46'E, 267 m a.s.l.), which is a ~110-year-old mixed stand of spruce (*Picea abies*, 61%), pine (*Pinus sylvestris*, 34%), and birch (*Betula*, 5%) (Laudon et al., 2013). Till and sorted sediments are the dominant soils at SVB. The mean tree height at SVB was 23.5 m on average. Both sites have a boreal climate with a long-term (1986-2015) mean annual temperature of 2.1°C and a mean annual precipitation of 619 mm (Laudon et al., 2013). The basal area is 27 and 30 m² ha⁻¹ and the stand density is 1010 ± 125 ha⁻¹ and 1152 ± 461 ha⁻¹ at ROS (Lim et al., 2015) and SVB, respectively. The leaf area index of 2.7 and 3.3 m² m⁻² for ROS and SVB, respectively, are relatively similar. However, the trunk space above the forest floor is more open at the pine stand ROS where canopy biomass is concentrated within the upper one-third of tree height, compared to SVB where spruce foliage and branches occurring along the entire stem create a denser near-surface trunk space (Fig. A1).

A forest floor inventory conducted at both sites (Supplemental Material S1) suggested that mosses were the dominant plant functional type and covered 55% and 38% of the floor surface at ROS and SVB, respectively (Figure S2). Dwarf shrubs (commonly 10-20 cm in height), i.e., bilberry (*Vaccinium myrtillus*) and lingonberry (*Vaccinium vitis-idaea*), account for 21% and 26% of the spatial coverage at ROS and SVB, respectively. Grass accounted for only < 10% of the floor surface at each site. Overall, the contribution of vascular plant (dwarf shrubs and grass) coverage was 12% greater at SVB compared to ROS.

2.2. Eddy covariance and ancillary measurements

Identical EC systems (CPEC 200, Campbell Scientific, Inc., USA) were installed at 2.5 m above the forest floor in the trunk space at ROS in June 2015 and SVB in September 2016. The EC systems consisted of a three-dimensional ultrasonic anemometer (CSAT3, Campbell Scientific, Inc., USA) for measuring wind components (*u*, *v*, and *w*) and sonic temperature (*T*), and a closed-path infrared gas analyzer (IRGA, EC155, Campbell Scientific, Inc., USA) for measuring CO₂ (*c*) and H₂O (*q*) concentrations. Both below-canopy EC systems sampled the raw data at a rate of 20 Hz. The above-canopy EC systems were installed at both sites to measure the ecosystem-scale CO₂ fluxes. At ROS, the above-canopy EC system was composed of a Gill R3-100 sonic anemometer (Gill

Instruments Limited, Hampshire, UK) and an LI-7200 infrared gas analyzer (LI-COR Biosciences, Lincoln, USA), installed 20.5 m above the ground in 2016 and raised to 21.5 m and 23.5 m in August 2017 and June 2019, respectively. At SVB, the above-canopy EC system consisted of a Gill HS-50 (Gill Instruments Limited, Hampshire, UK) sonic anemometer and an LI-7200 infrared gas analyzer (LI-COR Biosciences, Lincoln, USA). Until May 2018, the EC system was installed at 32.5 m above the ground and later on raised to 34.5 m.

Ancillary measurements were continuously recorded at 30-min intervals in the trunk space at both sites, including photosynthetic photon flux density (PPFD), air temperature (Ta), and relative humidity (RH) all measured 1.8 m above the ground, precipitation (PPT), soil temperature (Ts) at the depths of 15 and 50 cm, soil water content (SWC) at 15 (or 10) and 50 cm depths at ROS (SVB), and snow depth (SD). Vapor pressure deficit (VPD) was calculated from the 30-min Ta and RH measurements. Instrumentation of the ancillary measurements at the two sites is listed in Table S1. The long-term (1986-2019) weather data (i.e., daily Ta and PPT) were obtained from the Svartberget Hygget weather station (Laudon et al., 2013), which is located ~1.5 km away from the SVB flux tower and conforms with the standards defined by the World Meteorology Organization (WMO).

2.3. Study period

The below-canopy EC fluxes were measured during 2016-2019 and 2017-2019 for ROS and SVB, respectively. The above-canopy EC flux measurements were available during 2016-2019 and 2018-2019 at ROS and SVB, respectively. The annual period was defined as the calendar year, which was further divided into growing and non-growing seasons (GS and NGS, respectively). The GS start and end dates were defined as the first day with daily mean Ta > 5°C and < 5°C for five consecutive days, respectively. The remainder of each annual period was defined as NGS.

2.4. Flux calculation

2.4.1. Raw data processing

All the procedures involved in the below-canopy EC flux calculation are described in Fig. A2. The below-canopy EC raw data were processed using the EddyPro® software (v7.0.6, LI-COR Biosciences, USA) to obtain the half-hourly turbulent fluxes of momentum, sensible heat, CO₂, and H₂O. The 20 Hz raw data were filtered for abnormal diagnostic values of sonic anemometer and IRGA (i.e., the non-zero values). EddyPro was run following the ICOS data processing routine settings as described in Sabbatini et al. (2018), including double coordinate rotation for aligning the sonic anemometer with the local wind streamlines (Wilczak et al., 2001), block average for determining the turbulent fluctuations over each 30-min averaging period (Gash and Culf, 1996), and automatic time lag optimization for estimating the time lags between sonic anemometer and IRGA (Rebmann et al., 2012). The CO₂ and H₂O storage terms were calculated for each 30-min in EddyPro based on the one-level CO₂ and H₂O concentration measurements (Aubinet et al., 2001). Binned cospectra of sensible heat (*H*), CO₂, and H₂O fluxes were calculated for each 30-min period (Smith, 1997) and filtered for low data quality with the quality control flag equaling to 2 (Mauder and Foken, 2004) and based on statistical tests (Vickers and Mahrt, 1997) in EddyPro. However, the turbulent CO₂ and H₂O fluxes were not corrected for spectral attenuations via any of the approaches implemented in EddyPro, but were corrected afterward based on the typical cospectra patterns developed for the below-canopy EC measurements at each site (see Section 2.4.2).

The above-canopy EC raw data were processed using the same version of EddyPro, following the same routine data processing procedures as the below-canopy EC system. As the cospectra of CO₂ fluxes from the above-canopy EC systems matched well with the traditional cospectra model (Figure S3), spectral corrections for low-frequency

range were applied using the Moncrieff et al. (2004) approach at both sites and high-frequency range after Ibrom et al. (2007) at SVB and Moncrieff et al. (1997) at ROS.

2.4.2. Development of below-canopy spectral correction models

The below-canopy turbulence differs significantly from the above-canopy; for example, more fine-scale eddies may occur due to wake production surrounding the foliage parts (Finnigan, 2000). Consequently, the traditional above-canopy cospectra model cannot reflect the actual turbulence distribution in the trunk space and thus may lead to biased flux estimates. Below-canopy cospectra models are the pre-requisite for improving the accuracy of flux estimates. To develop the below-canopy cospectra models, the half-hourly binned cospectra data obtained from EddyPro were further filtered for low turbulence and noise contamination. Following Launiainen et al. (2005), the standard deviation of the vertical wind speed (σ_w) was used to identify the turbulent and unstable conditions, which has also been applied to filter fluxes in most of the below-canopy EC studies (Jocher et al., 2017; Kulmala et al., 2008; Kulmala et al., 2019; Lindroth et al., 2018; Paul-Limoges et al., 2017; Paul-Limoges et al., 2020; Thomas et al., 2013). Data within the σ_w ranges of 0.2-0.35 m s⁻¹ and 0.15-0.25 m s⁻¹ at ROS and SVB, respectively, were identified as measurements under the highly turbulent condition and thus selected for fitting the cospectra curves. As expected, the turbulent CO₂ flux variations were small and the CO₂ storage terms were close to zero when σ_w was within the selected ranges (Figure S4). Besides, a linear fit of the inertial subrange (normalized frequency > 1) was performed on the log-log cospectra curve to select the noise-free measurement periods (Figure S5). Theoretically, a slope of -4/3 for the inertial subrange frequency is expected in the cospectra of surface-layer turbulence (Kaimal et al., 1972) and values between 0 to 1 were considered as partial noise within that frequency range (Stull, 1988). Therefore, we removed the noise-contaminated cospectra when the fitted slope was greater than zero, as suggested in Falk et al. (2005).

Spectral attenuations (e.g., high-frequency loss) typically occur for the CO₂ and H₂O fluxes due to signal losses in the sampling line and sensor separation for a closed-path EC system. We thus only used the high-quality cospectrum density of sensible heat flux (C_{wr}) to fit the site-specific cospectra curves by adjusting the traditional model (Eq. 1) that was developed for the above-canopy EC measurements (Kaimal et al., 1972).

$$\frac{f C_{wr}(f)}{w'T} = \frac{an}{(1+bn)^c} n = \frac{f(z-d)}{U} \quad (1)$$

where f is the natural frequency ranging from 1/1800 to 10 Hz in this study, z is the EC measurement height (2.5 m), d is the displacement height (m) estimated as two-thirds of understory canopy height (0-0.12 m), U is the 30-min mean wind speed (m s⁻¹), n is the dimensionless normalized frequency, and abc are the model parameters. According to Kaimal et al. (1972), model parameters were fitted for two frequency ranges ($n < 0.54$ and $n \geq 0.54$).

The site-specific fitted cospectra curves represented the typical turbulence characteristics ideal for the below-canopy EC measurements, which were therefore applied as the cospectra models to correct the turbulent CO₂ and H₂O fluxes for each 30-min averaging period. The half-hourly correction factor (CF), defined as the ratio between the real (r) and measured (m) flux (Moore, 1986), was calculated as the ratio between the integrated modeled and measured cospectra (Eq. 2).

$$CF = \frac{(\overline{w's})_r}{(\overline{w's})_m} = \frac{\int_0^\infty C_{ws}(f)_r df}{\int_0^\infty C_{ws}(f)_m df} \quad (2)$$

where s represents the scalar variable of T , c , or q in H , CO₂, or H₂O fluxes, respectively. The uncorrected turbulent fluxes were multiplied by the CF and then added to the storage terms to obtain the net forest floor

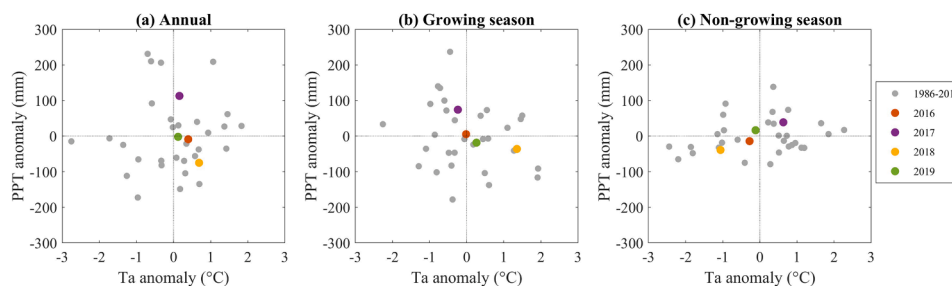


Fig. 1. Annual (a), growing season (b), and non-growing season (c) anomalies of air temperature (Ta) and precipitation (PPT) during the study years 2016–2019. Anomalies are relative to the 30-year (1986–2015) mean Ta and PPT for annual, growing season, non-growing season, respectively. Data are from the Svartberget Hygget weather station located close to the SVB flux tower.

exchange of CO₂ (NFFE) and H₂O (data not shown in this study). In this study, the micrometeorological sign convention was used that negative and positive CO₂ fluxes indicate uptake by and emission from the forest floor, respectively.

2.4.3. Data quality control

The half-hourly NFFE was further filtered for the following quality assurance/quality control (QA/QC) criteria: plausible NFFE range of -50 to 50 $\mu\text{mol m}^{-2} \text{s}^{-1}$, low data quality (EddyPro qc flagging “2”) (Mauder and Foken, 2004), spikes accounting for more than 1% of raw data for each 30-min averaging period (Paul-Limoges et al., 2017), slope of the inertial subrange greater than zero (Falk et al., 2005), advection occurrence when the horizontal and vertical mean flows become dominant over turbulence (Wharton et al., 2009), statistical outliers outside the range of mean $\pm 3 \times$ standard deviation, sensor malfunctioning, and site disturbances. Following Paul-Limoges et al. (2020), we also filtered NFFE measured under the condition of counter-gradient transport, i.e., flagging NFFE for the negative water fluxes which were caused by the downward eddies while the below-canopy air temperature was above the dew point temperature. This counter-gradient transport condition occurred in 18% and 13% of the measurement period at ROS and SVB, respectively. The correction for counter-gradient transport slightly decreased the mean annual NFFE by 14 and 2 $\text{g C m}^{-2} \text{yr}^{-1}$ at ROS and SVB, respectively. As the storage and advection terms have been taken into account, neither σ_w nor other stability parameters were applied for data-filtering. Over the three (or four) years, 46% and 53% of the half-hourly NFFE data were identified as good quality data at ROS and SVB, respectively.

The above-canopy EC fluxes were filtered for periods with weak turbulent mixing when the air flows were decoupled from the below-canopy (Jocher et al., 2017), indicated by the non-linear relationship between the below- and above-canopy σ_w (Figure S6). As the decoupling effects on the above-canopy EC measurements at the ROS site have been previously investigated in Jocher et al. (2017) and Jocher et al. (2018), this study illustrated the effects of different filtering strategies (i.e., σ_w and u_*) on annual NEE for the SVB site only (Table S2). At ROS and SVB, 48.8% and 48.9% of the half-hourly NEE data were left for the above-canopy flux measurements, respectively. Periods with concurrent data for above- and below-canopy EC fluxes accounted for 28% and 21% of the entire datasets at ROS and SVB, respectively.

2.4.4. Flux gap-filling and partitioning

Gaps in the half-hourly NFFE were filled using the marginal distribution sampling (MDS) approach (Reichstein et al., 2005) implemented in the REdDyProc online tool (Wutzler et al., 2018). The gap-filled NFFE was partitioned into total respiration and gross primary production of the forest floor, R_{ff} and GPP_{ff} , respectively, through estimating R_{ff} using the conditional sampling approach (Thomas et al., 2008). The R_{ff} term defined in this study includes tree and understory vegetation root respiration, heterotrophic respiration, and understory vegetation autotrophic respiration. A detailed description of R_{ff} estimates was described

in Jocher et al. (2017), which calculates the covariance (5-min averaging intervals) between w' and c' only for positive vertical winds. As a modification of the conditional sampling method, a respiration-evaporation cluster was detected for each averaging period and data within the cluster were sampled to estimate R_{ff} (Klosterhalfen et al., 2019). The 5-min averaged R_{ff} was resampled to the 30-min mean, which was then filtered for the same QA/QC criteria listed in Section 2.4.3. Gaps in the half-hourly R_{ff} were filled using the empirical respiration model (Eq. 3) fitted by the filtered R_{ff} and T_s every year (Barr et al., 2004).

$$R_{ff} = f(T_s, t) = \frac{r_w(t)r_1}{1 + \exp[r_2(r_3 - T_s)]} \quad (3)$$

where r_1 , r_2 , and r_3 are empirical constants, $r_w(t)$ is an additional parameter that described the difference between the measured and modeled R_{ff} at time t , and T_s is the soil temperature measured at a depth of 15 cm. Finally, GPP_{ff} was estimated as NFFE minus R_{ff} for each half-hour. However, GPP_{ff} was forced to zero with R_{ff} equaling NFFE when Ta was below -5°C , or the below-canopy PPFD was less than $65 \mu\text{mol m}^{-2} \text{s}^{-1}$ where photosynthesis of the forest floor vegetation was considered negligible (Figure S7). It should be noted that different flux partitioning approaches provided various R_{ff} estimates (Figure S8), but the conditional sampling based approach showed fewer artifacts in the partitioned fluxes (e.g., positive monthly GPP_{ff} sums, no physical meaning) compared to the nighttime-based (Reichstein et al., 2005), daytime-based (Lasslop et al., 2010), and modified daytime-based (Keenan et al., 2019) partitioning methods (Figures S9 and S10). The above-canopy EC fluxes, i.e., net ecosystem exchange of CO₂ (NEE), were filled using the MDS method and partitioned into ecosystem respiration (R_{eco}) and gross primary production (GPP) using the commonly applied nighttime-based approach (air temperature as the R_{eco} driver) in the REdDyProc online tool.

2.4.5. Uncertainty and statistical analysis

Monte Carlo simulations (100 repetitions) were performed to assess the uncertainty in annual NEE and NFFE sums due to gap-filling (Table S3), following the procedures described in Richardson and Hollinger (2007). Random errors were added to the half-hourly non-gapfilled datasets, which were drawn from a Laplace distribution reported in Richardson and Hollinger (2005) for NEE and a newly fitted Laplace distribution for NFFE from this study (Figure S11).

Principle component analysis (PCA) was performed on the half-hourly measured data (non-gapfilled) to investigate the relationships between the forest floor CO₂ fluxes and the environmental variables during the growing and non-growing seasons, respectively. Response curves of CO₂ fluxes to environmental controls were fitted and evaluated by the coefficient of determination (R^2) and root mean square error (RMSE).

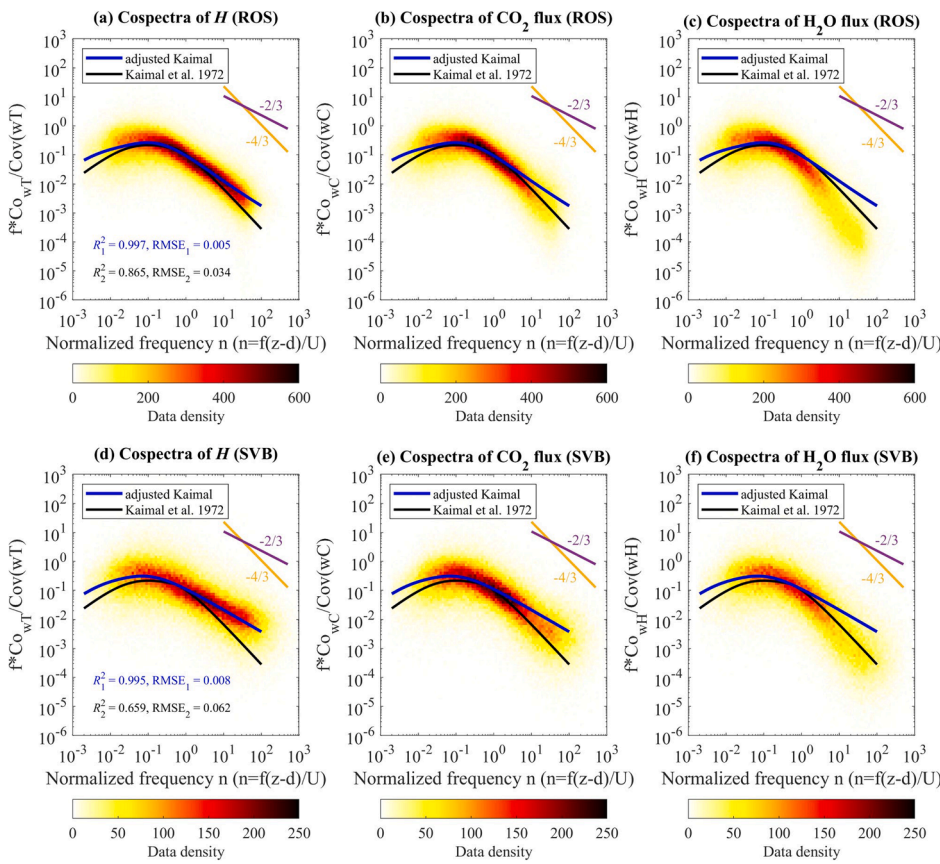


Fig. 2. Typical cospectra curves (blue lines) for the below-canopy EC measurements at ROS (a-c) and SVB (d-f). The color of the heat map reflects the data density of the 30-min binned cospectra data of H (a, d), CO_2 (b, e), and H_2O (c, f) fluxes selected for the highly turbulent and noise-free conditions. Black lines are the traditional cospectra model from Kaimal et al. (1972). Yellow and purple lines represent the slope values of $-4/3$ and $-2/3$, respectively. The coefficient of determination (R^2) and root mean square error (RMSE) of the model performance is labeled in the cospectra of H panels (a, d) where blue and black fonts represent the model performance of our below-canopy cospectra model and the traditional model, respectively.

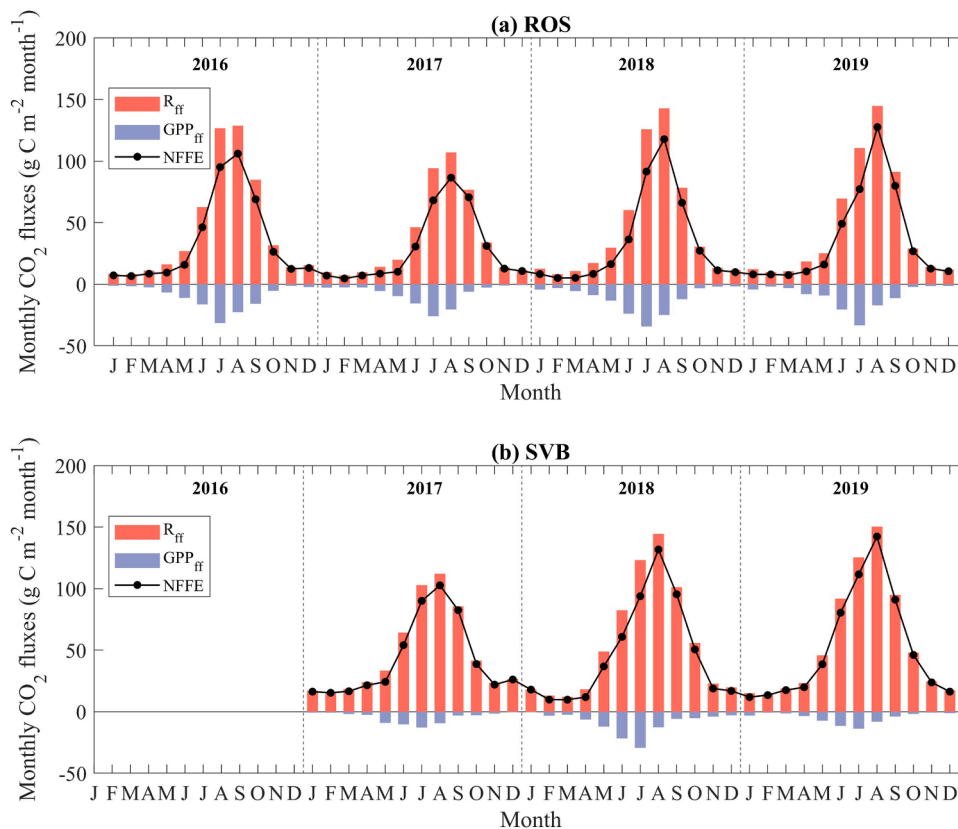


Fig. 3. Monthly sums of forest floor net CO_2 exchange (NFFE), gross primary production (GPP_{ff}), and total respiration (R_{ff}) at ROS (a) and SVB (b) during the study periods of 2016-2019 and 2017-2019, respectively.

Table 1
Growing season (GS) and non-growing season (NGS) forest floor CO₂ budgets at ROS and SVB

Year	NFFE (g C m ⁻²)				GPP _{ff} (g C m ⁻²)				R _{ff} (g C m ⁻²)			
	GS		NGS		GS		NGS		GS		NGS	
	ROS	SVB	ROS	SVB	ROS	SVB	ROS	SVB	ROS	SVB	ROS	SVB
2016	341	n/a	75	n/a	-101	n/a	-18	n/a	442	n/a	93	n/a
2017	277	359	71	152	-74	-43	-23	-13	351	402	93	165
2018	330	418	73	137	-113	-85	-25	-21	443	503	98	158
2019	332	443	102	170	-92	-45	-22	-12	424	488	124	182

3. Results

3.1. Environmental conditions

Within the four-year study period, 2017 was the wettest and 2018 the driest year, receiving 113 mm more and 75 mm less PPT than the 30-year mean annual PPT, respectively (Fig. 1a). More specifically, the 2017 growing season (GS) was cool and wet in contrast to the hot and dry GS during 2018 (Fig. 1b). However, the 2017 non-growing season (NGS) was the warmest and wettest, and 2018 had the coldest and driest NGS among the four years (Fig. 1c). During the years of 2016 and 2019, the weather conditions were close to the long-term averaged records during both GS and NGS (Fig. 1).

3.2. Below-canopy cospectra models

The fitted cospectra curves using the sensible heat flux cospectra data under the turbulent and noise-free conditions represented the empirical below-canopy cospectra models (Fig. 2). Our below-canopy models showed that more low- and high-frequency signals occurred in the forest trunk space compared to the ideal above-canopy cospectra model from Kaimal et al. (1972). The difference between below- and above-canopy cospectra was more pronounced in the dense spruce-pine forest SVB compared to the open pine stand ROS (Fig. 2a and 2d). The inertial subrange slope in the fitted cospectra curve did not follow the theoretical value of -4/3 but was closer to -2/3 at both sites.

Compared to the traditional cospectra model from Kaimal et al.

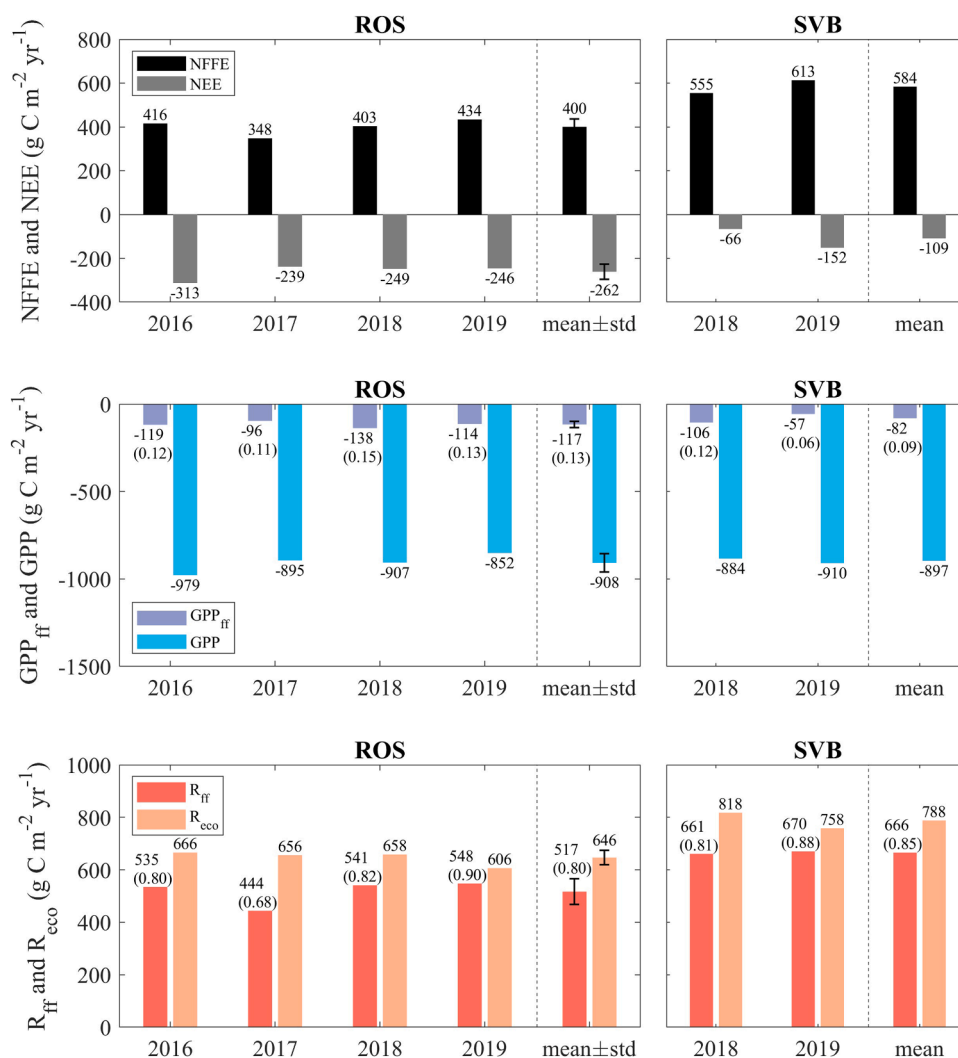


Fig. 4. Annual sums of the CO₂ fluxes of the forest floor (NFFE, GPP_{ff}, and R_{ff}) and the forest ecosystem (NEE, GPP, and R_{eco}) at ROS (2016-2019) and SVB (2018-2019). Numbers in parentheses represent the GPP_{ff}/GPP and R_{ff}/R_{eco} ratios.

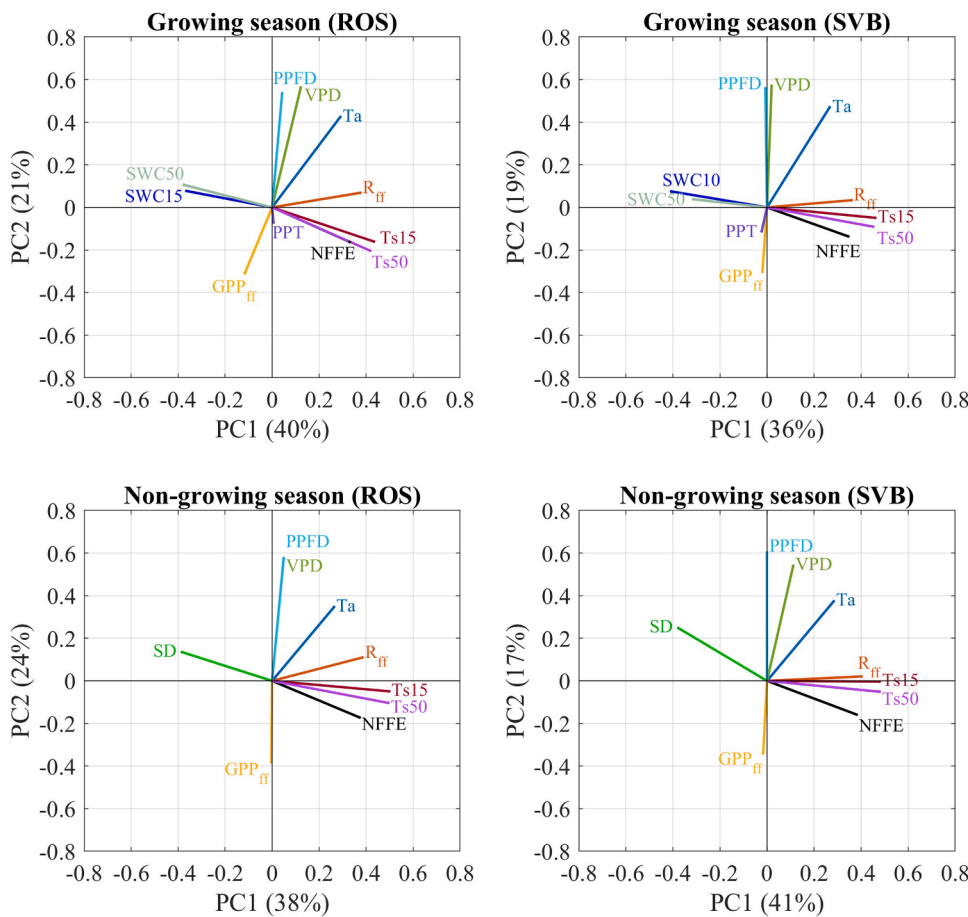


Fig. 5. PCA loading plots of the correlation structures of the half-hourly forest floor CO₂ fluxes (NFFE, GPP_{ff}, and R_{ff}) and environmental variables during growing and non-growing seasons at ROS and SVB. Environmental variables include below-canopy photosynthetic photon flux density (PPFD), air temperature (Ta), vapor pressure deficit (VPD), precipitation (PPT), soil temperature at the depths of 15 and 50 cm (Ts₁₅ and Ts₅₀), soil water content (SWC) at two depths (15 and 50 cm for ROS; 10 and 50 cm for SVB), and snow depth (SD).

(1972), our empirical cospectra models showed a better fit to the *H* cospectra data with a higher coefficient of determination (R^2 , 0.997 and 0.995 vs. 0.865 and 0.659) and a smaller root mean square error (RMSE, 0.005 or 0.008 vs. 0.034 or 0.062). Moreover, the traditional cospectra model suggested no apparent spectral loss in the CO₂ and H₂O fluxes (Fig. 2b, 2c, 2e, and 2f). However, referring to our site-specific cospectra models, the expected spectral attenuations due to sensor separations and losses in the sampling line were noted again in the high-frequency range for CO₂ and H₂O fluxes at both sites (Fig. 2b, 2c, 2e, 2f), with more H₂O signal loss compared to the CO₂ flux frequency loss because of the ‘sticky’ nature of the H₂O molecules. After applying our empirical cospectra models to correct the turbulent fluxes, the averaged correction factors for CO₂ and H₂O fluxes at ROS were 1.24 and 1.28, respectively, which were both smaller compared to the factors at SVB, i.e., 1.44 and 1.46 for CO₂ and H₂O, respectively. In the following study, we used our cospectra-corrected CO₂ fluxes to analyze the seasonal and inter-annual variability of forest floor CO₂ budgets, their contributions to the ecosystem-scale C budgets, and flux responses to environmental conditions in the following results and discussion sections.

3.3. Seasonal and inter-annual variability of forest floor CO₂ fluxes

The monthly sums of NFFE showed that the forest floor was a net CO₂ source for all months throughout the entire study period at both sites (Fig. 3). For all years, the peak monthly NFFE (i.e., net CO₂ emission) and R_{ff} occurred in August, while the peak GPP_{ff} was found to be in July persistently. Both sites showed a similar inter-annual variation of the growing season (GS) forest floor CO₂ flux sums (Table 1). The lowest GS sums of GPP_{ff} and R_{ff} during 2017 concurred with the coolest and wettest environmental conditions, whereas both GS sums of GPP_{ff} and R_{ff} were higher in the warmer and drier years of 2016, 2018, and 2019

(Table 1, Fig. 1). As the increase in the GPP_{ff} flux magnitude was smaller than that of R_{ff} during the warmer and drier years, the GS sums of NFFE were more positive during 2016, 2018, and 2019 with the highest value being recorded in 2016 at ROS and 2019 at SVB.

The non-growing season (NGS) sums of NFFE accounted for 0.18–0.30 fractions of the annual NFFE (Table 1). However, the two sites showed different inter-annual variations of NGS sums of NFFE (or R_{ff}). At ROS, the NGS sums of NFFE (or R_{ff}) did not differ much from 2016 to 2018, with the highest value being recorded in 2019 (Table 1). Whereas at SVB, the NGS sums of NFFE (or R_{ff}) corresponded with the inter-annual variation of NGS air temperature (Table 1, Fig. 1c). Overall, the NGS sums of NFFE at SVB exceeded ROS by $71 \pm 9 \text{ g C m}^{-2}$, which was comparable to their difference in the GS sums ($94 \pm 15 \text{ g C m}^{-2}$).

Over each annual cycle, R_{ff}, rather than GPP_{ff}, was the dominant flux component that positively affected NFFE variations, with a stronger correlation between R_{ff} and NFFE at SVB than at ROS (Figs. 4 and 5). Both sites showed similar inter-annual variabilities of the forest floor CO₂ yearly budgets (Table 1, Fig. 4). From 2017 to 2019, the annual NFFE increased by 12% and 10% per year at ROS and SVB, respectively. The 2016 NFFE at ROS was slightly greater than the 4-year mean. At ROS and SVB, the largest annual GPP_{ff} occurred in 2018; and the annual R_{ff} during 2018 and 2019 had similar magnitudes, which were higher than the years of 2016 (ROS only) and 2017. Compared to the mean annual NFFE during 2017–2019 at ROS ($395 \pm 44 \text{ g C m}^{-2} \text{ yr}^{-1}$), the forest floor at SVB acted as a stronger net CO₂ source ($560 \pm 51 \text{ g C m}^{-2} \text{ yr}^{-1}$) due to the on average 1.2 times higher R_{ff} and GPP_{ff} constituting 0.63 fraction of GPP_{ff} at ROS.

3.4. Forest floor flux contributions to the ecosystem-scale C budgets

The annual GPP_{ff}/GPP ratios did not differ much among the four

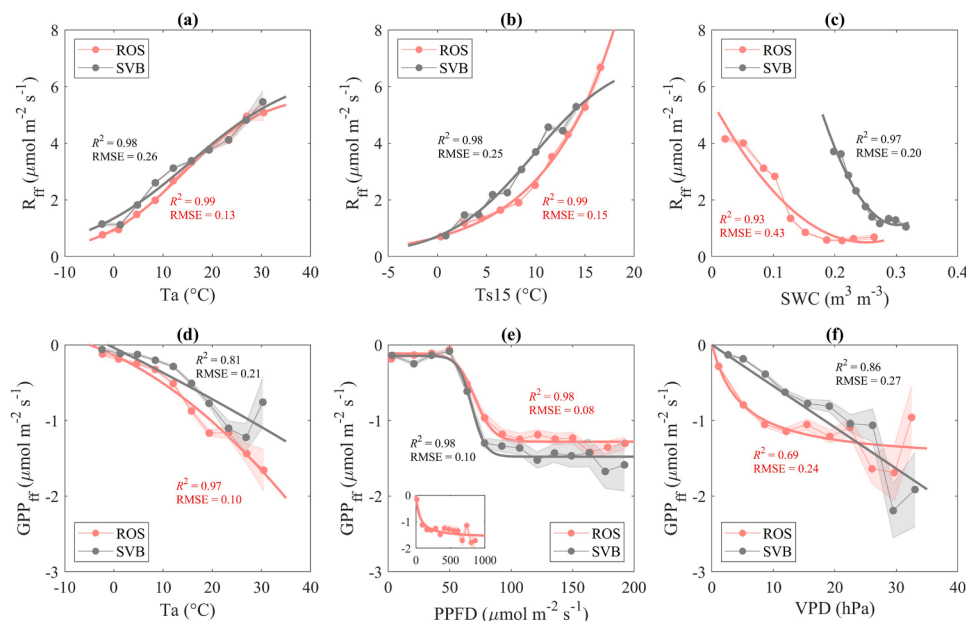


Fig. 6. Bin-averaged half-hourly forest floor CO_2 fluxes (R_{ff} and GPP_{ff}) vs. their abiotic controls during the 2017-2019 growing seasons at each site. Abiotic controls include below-canopy air temperature (T_a) measured at 1.8 m above the ground, soil temperature measured at a depth of 15 cm (T_{s15}), soil water content (SWC) measured at the depths of 15 cm and 10 cm at ROS and SVB, respectively, below-canopy photosynthetic photon flux density (PPFD) measured at 1.8 m above the ground and vapor pressure deficit (VPD) calculated from the T_a and RH measurements at 1.8 m above the ground. The zoom-out plot in panel (e) is GPP_{ff} vs. PPFd with coarser bins in the PPFd range of 0-1000 $\mu\text{mol m}^{-2} \text{s}^{-1}$ at ROS. Shaded areas represent the standard errors of the bin averages. The solid red and grey lines are the fitted response curves to the environmental controls for R_{ff} and GPP_{ff} at ROS and SVB, respectively. The coefficient of determination (R^2) and root mean square error (RMSE) of the fitted curves are labeled in each panel.

years at ROS within the range of 0.11-0.15, whereas R_{ff}/R_{eco} ratios showed a larger inter-annual variability ranging from 0.68 to 0.90 (Fig. 4). At ROS, the forest floor contributions to the ecosystem-scale GPP and R_{eco} were high in 2018 and 2019, whereas the lowest contributions occurred in the coolest year 2017. Contrasting to ROS, the annual GPP_{ff}/GPP ratio at SVB was reduced by 50% from 2018 to 2019, but the annual R_{ff}/R_{eco} ratio varied by only 0.07 between the two years. At SVB, the averaged GPP_{ff}/GPP and R_{ff}/R_{eco} ratios over the two years of 2018 and 2019 were 0.09 and 0.85, respectively, similar to the values of 0.14 and 0.86 at ROS over the same two years (Fig. 4).

The ecosystem-scale C budgets suggested that both forests were net CO_2 sinks for all years of the study period (Fig. 4). During the years of 2018 and 2019 with data from both sites, the annual net CO_2 uptake at ROS ($-248 \text{ g C m}^{-2} \text{ yr}^{-1}$) was more than twice as high as at SVB ($-109 \text{ g C m}^{-2} \text{ yr}^{-1}$). This difference resulted from the $\sim 25\%$ lower R_{eco} and nearly identical GPP (Fig. 4). Correspondingly, the mean annual R_{ff} at ROS was $\sim 22\%$ lower than at SVB during the same two years. Furthermore, at a higher temporal resolution, the daily R_{ff} explained 84% and 88% of the daily R_{eco} variances at ROS and SVB, respectively (Figure S12). As the R_{ff} and R_{eco} were the dominant flux components that determined the variations of NFFE and NEE, respectively, NFFE was identified as the main driving factor of the NEE difference between the two forest stands.

3.5. Abiotic controls of forest floor CO_2 fluxes

At both sites, R_{ff} showed a positive correlation with soil temperature (T_s) throughout the year but correlated negatively with soil water content (SWC) during the growing season and with snow depth (SD) during the non-growing season (Fig. 5). The below-canopy PPFd, T_a , and VPD were positively correlated with understory photosynthesis rates (i.e., negative GPP_{ff}) at each site (Fig. 5).

The bin-averaged response of R_{ff} to T_a demonstrated that R_{ff} increased with T_a at both sites with a similar T_a sensitivity, forming a slight plateauing pattern when $T_a > 30^\circ\text{C}$ (Fig. 6a). However, the dependence of R_{ff} on T_s variations differed at the two sites: R_{ff} increased more rapidly at high T_s range ($> 10^\circ\text{C}$) at ROS, whereas R_{ff} at SVB responded more sensitively in low T_s range ($< 10^\circ\text{C}$) (Fig. 6b). Moreover, R_{ff} decreased with the rising SWC but remained constant when $\text{SWC}_{15} > 0.15 \text{ m}^3 \text{ m}^{-3}$ and $\text{SWC}_{10} > 0.27 \text{ m}^3 \text{ m}^{-3}$ at ROS and SVB, respectively (Fig. 6c). As R_{ff} was the dominant flux component of NFFE, correlations of the environmental variables with the latter were similar

to those of R_{ff} .

Unlike the similar responses of R_{ff} to T_a at the two sites, GPP_{ff} was more enhanced with the increased T_a at ROS compared to SVB (Fig. 6d). The smaller magnitudes of GPP_{ff} (less negative values) at the high T_a range at SVB constrained the response curve to a large divergence from ROS, which however remained uncertain due to the limited number of data points at the high T_a range and the GPP_{ff} uncertainty resulting from the partitioning approach. Significant increases in GPP_{ff} at the open forest ROS were identified within the below-canopy PPFd range of 65-500 $\mu\text{mol m}^{-2} \text{ s}^{-1}$, beyond which GPP_{ff} started approaching light saturation with a maximum CO_2 uptake capacity of $1.6 \mu\text{mol m}^{-2} \text{ s}^{-1}$ (Fig. 6e). However, GPP_{ff} was limited by the below-canopy PPFd at the dense forest SVB, as the maximum below-canopy PPFd was up to 200 $\mu\text{mol m}^{-2} \text{ s}^{-1}$ (Fig. 6e). The relationship between GPP_{ff} and VPD showed that the understory vegetation photosynthesis generally increased as VPD increased up to a VPD threshold of $\sim 30 \text{ hPa}$ beyond which GPP_{ff} started to decrease (Fig. 6f).

4. Discussion

4.1. Turbulence characteristics in the trunk space of two contrasting forests

Our study highlights the need for distinct below-canopy cospectra models as our results showed that the classic above-canopy model may introduce bias into the below-canopy EC measurements. The increased distributions of low-frequency turbulence (i.e., large-scale eddies) observed in the trunk space at both open and dense forests may result from fast gusts moving downward (i.e., sweeps) from above-canopy into the trunk space (Finnigan, 2000). Due to the small fractions of occurrence, the counter-gradient transport associated with the downward fast gusts did not affect the low-frequency turbulence distribution illustrated in the below-canopy cospectra curves. Meanwhile, the interaction of the airflow with the trunks, branches, and leaves may increase fine-scale turbulence (i.e., high-frequency) in the wakes of the canopy elements (e.g., Brunet, 2020; Finnigan, 2000). Without recognizing the differences between below- and above-canopy cospectra models, the comparable pattern of CO_2 and H_2O flux cospectra to the traditional above-canopy cospectra model may be falsely interpreted as satisfactory below-canopy eddy covariance measurements. Consequently, the high-frequency signal attenuation in the sampling line of closed-path EC

can be considerably masked by the traditional above-canopy cospectra model if applied to below-canopy EC data, resulting in underestimated forest floor fluxes in dense forest (Figure S13).

Both sweeps and wake production commonly play a greater role in dense than in sparse canopies (Poggi et al., 2004; Russell et al., 2018). Therefore, the effects of tree species and stand density on low- and high-frequency turbulent eddies were more pronounced at SVB, where the forest was denser and more branches and foliage located in the lower part of the spruce trees compared to the open pine forest ROS. Compared to the traditional (Moncrieff et al., 1997) and previous *in-situ* spectral correction approaches (e.g., Fratini et al., 2012), the method proposed in this study successfully addressed the distinct site-specific effects on the below-canopy flux measurements and forest floor annual CO₂ budgets. For example, applying the traditional cospectra model resulted in comparable annual CO₂ fluxes (4%, 15 g C m⁻² yr⁻¹) at the open pine stand but significantly underestimated the annual CO₂ fluxes by 14% (74 g C m⁻² yr⁻¹) at the dense spruce-pine forest (Figure S13). Therefore, our results further indicate that the below-canopy cospectra models need adaptation to site-specific canopy conditions.

4.2. Seasonal and annual forest floor CO₂ budget differences across contrasting sites

The annual net CO₂ source strength of the forest floor 400 ± 37 and 560 ± 51 g C m⁻² yr⁻¹ from ROS (2016-2019) and SVB (2017-2019) respectively estimated in this study was within the wide range of 250-1360 g C m⁻² yr⁻¹, reported in previous studies in the boreal region (Black et al., 1996; Gaumont-Guay et al., 2014; Launiainen et al., 2005; Morén and Lindroth, 2000; Swanson and Flanagan, 2001; Widén, 2002). Compared to the ROS pine forest in 2017-2019, the forest floor CO₂ source strength at the SVB spruce-pine forest was 1.4 times stronger and attributed to the higher forest floor respiration accompanied by the lower understory photosynthesis.

As tree root respiration is strongly determined by the photosynthate C allocation (Bhupinderpal-Singh et al., 2003; Högberg et al., 2001), the autotrophic root respiration during the growing season (GS) may be comparable between the two sites due to their similar GPP magnitudes, assuming the same below-ground C allocation pattern at ROS and SVB. Therefore, the NFFE difference between the two sites might be mainly attributed to the heterotrophic respiration component during both GS and NGS. At SVB, the higher deadwood decomposition rates reported for spruce (Shorohova et al., 2008) and larger litterfall C input might contribute to the higher heterotrophic respiration than the pine stand. Besides, the soil organic layer is thicker at SVB (10-15 cm) than at ROS (2-5 cm) (Hasselquist et al., 2012; Laudon et al., 2011), which can be assumed to contribute to the higher soil heterotrophic respiration at SVB.

As the photosynthetic activity of the forest floor is strongly light-limited (e.g., Kulmala et al., 2011; Misson et al., 2007), the lower photosynthesis at the dense SVB forest may be the result of the reduced amount of light penetrating onto the forest floor, compared to the open trunk space at ROS. Therefore, the site characteristics (e.g., canopy structure, tree and understory species composition and biomass production, and soil properties) significantly affected the forest floor CO₂ budgets by altering the C allocation patterns, microclimate, and soil biological processes.

4.3. The role of forest floor CO₂ fluxes in the ecosystem-scale C budget

Our results demonstrate that the tree CO₂ uptake (i.e., as GPP-GPP_{ff}) in two boreal coniferous stands was the dominant sink for atmospheric CO₂, while the contribution of understory vegetation photosynthesis to the ecosystem-scale GPP was limited. Our GPP_{ff}/GPP estimates were also close to the lower band of the wide range of 2-61%, which have been previously reported for the boreal forests (Bergeron et al., 2009; Ikawa et al., 2015; Ilvesniemi et al., 2009; Kolari et al., 2006; Kulmala

et al., 2011; Misson et al., 2007; Palmroth et al., 2019; Swanson and Flanagan, 2001).

The contribution of forest floor respiration to the total ecosystem respiration observed in our study was close to the higher end of the range of 40-90% estimated for other boreal forests (Bergeron et al., 2009; Black et al., 1996; Goulden and Crill, 1997; Ikawa et al., 2015; Launiainen et al., 2005; Morén and Lindroth, 2000; Shibistova et al., 2002). The stem and foliage respiration estimated as R_{eco} minus R_{ff}, accounting for 10-32% of R_{eco} at our pine stand, compares with 39% of R_{eco} estimated in a 200-year-old Scots pine stand in central Siberia (Shibistova et al., 2002) and 15-45% of R_{eco} reported in a temperate 70-year-old white pine (*Pinus strobus* L.) forest in Canada (Peichl et al., 2010). However, the stem and foliage respiration might be slightly underestimated in this study because R_{ff} measured using the EC method includes small fractions of the autotrophic respiration from stems, branches, foliage, and seedlings existing in the lower part of the forest below the EC mounting height (2.5 m), which is however likely small compared to the forest floor contribution (Tarvainen et al., 2017). The maximum R_{ff} contribution (90%) to R_{eco} during 2019 at ROS appears high and is likely an overestimation due to a one-month gap in the below-canopy EC data that resulted in increased uncertainty in R_{ff} during that year. Moreover, we found that the R_{ff} contribution to R_{eco} varied within about 10-15% depending on dominant wind sectors (Figure S14). Thus, the spatial heterogeneity of forest floor and tree stands into different wind directions may also result in variations and uncertainty when estimating the forest floor contributions to the ecosystem-level C budgets.

As the ecosystem GPP did not differ significantly between the two sites, their NEE difference was related to differences in R_{eco} magnitudes. R_{eco} itself however was strongly regulated by NFFE (or R_{ff}), which implies that the forest floor component essentially determined the difference in annual NEE between these two contrasting boreal forest stands. This finding highlights that the net forest floor CO₂ budget may act as the driving factor determining the variation of ecosystem-scale CO₂ balances across boreal forest stands within a given climatic region and stand developmental stage. This study also demonstrates the potential role of the forest floor in explaining the spatial variability of forest C budgets among mature stands within the boreal region. Thus, extending our efforts in acquiring comprehensive data on forest floor CO₂ fluxes (i.e., by the use of EC) will be critical for improving our understanding of the contributions from various ecosystem components to the forest C balance.

4.4. Sensitivity of forest floor CO₂ fluxes to environmental conditions and global change

Soil temperature as the dominant abiotic control of NFFE has been widely reported in other understory studies (Black et al., 1996; Gaumont-Guay et al., 2014; Kelliher et al., 1999; Kulmala et al., 2008; Launiainen et al., 2005). Our results further highlight that the net CO₂ source strength of the boreal forest floor may become enhanced during drought years as in 2018, mostly due to the elevated forest floor respiration under the warm conditions. As low soil moisture typically inhibits the organic matter decomposition (Manzoni et al., 2012), our observed increase in forest floor respiration under dry soil conditions may primarily result from the simultaneous increases in soil temperature and thus heterotrophic respiration rates (Bhupinderpal-Singh et al., 2003). Due to its large contribution to ecosystem respiration, our study further concludes that the forest floor was driving the ecosystem respiration responses to the drought event.

Although photosynthesis of the understory vegetation was also enhanced by the rising air temperature during 2018, it compensated the elevated forest floor respiration only to a small extent during the drought year. Furthermore, GPP_{ff} inhibition under high VPD (e.g., VPD > 30 hPa) indicates that the stomata of the vascular understory vegetation (i.e., dwarf shrubs and grass) might shut down to prevent



Fig. A1. The below-canopy eddy covariance tower set-up at ROS (a) and SVB (b) sites.

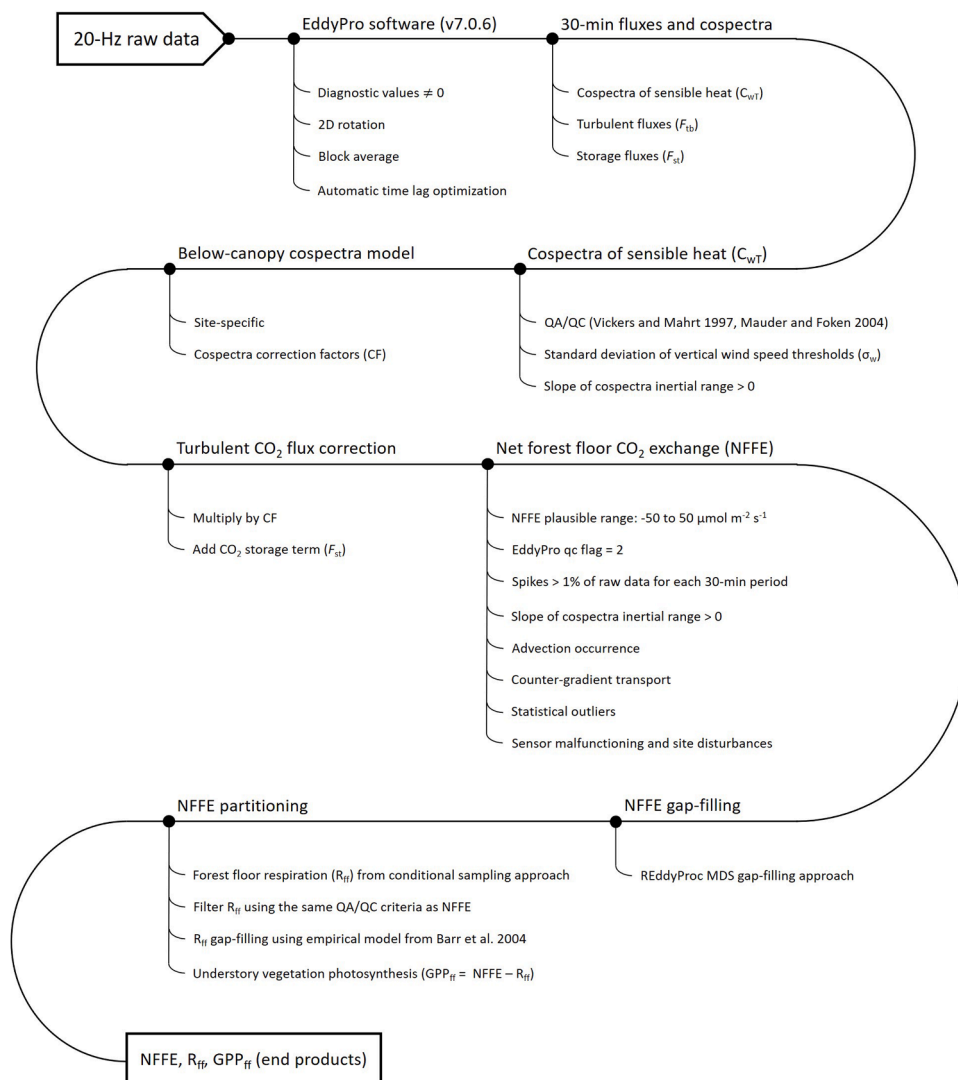


Fig. A2. Workflow of the below-canopy eddy covariance flux calculation.

extensive water loss into the atmosphere (Ikawa et al., 2015; Palmroth et al., 2019). The negative feedback to the high atmospheric water demand may become more pronounced at the forest floor with more vascular canopy distributions. Since the frequency and severity of drought events (including both air and soil conditions) might increase in the future (Allen et al., 2010), the photosynthesis of understory vegetation and the entire ecosystem might be reduced and the respiration components (e.g., forest floor respiration) might become the more prominent processes. Hence the forest floor is likely to become even more important in regulating the C balance of boreal forest ecosystems under future climate change.

Recent studies have extensively focused on the year 2018, during which the hot and dry summer conditions may have considerably altered the C balance in European terrestrial ecosystems (e.g., Lindroth et al., 2020; Peters et al., 2020). However, our study demonstrates that the annual forest floor net CO₂ source strength was even greater in 2019 than in 2018, as the ~1°C warmer soil during the 2019 non-growing season (NGS) resulted in higher forest floor respiration than during the 2018 NGS. This highlights the significant effects of the NGS environmental conditions on the annual forest floor CO₂ fluxes and their contributions to the ecosystem-scale C balance, which usually cannot be accounted for in chamber-based studies. As autumn and winter warming might continue in the studied region until 2090, the end of the simulation period in Teutschbein et al. (2015), we need to improve our understanding of non-growing season forest floor CO₂ budgets, especially in the high-latitude studies as previously suggested in other cold regions (Aurela et al., 2002; Commane et al., 2017; Natali et al., 2019). This calls for a more extended application of the EC technique for year-round measurements of the forest floor CO₂ exchange.

5. Conclusions

Our study shows that the classic above-canopy cospectra model may introduce bias in below-canopy eddy covariance measurements, particularly in a dense forest stand. Thus, we propose the need for empirical below-canopy cospectra models adapted to site-specific canopy conditions to improve eddy covariance flux measurements over the forest floor. Our study demonstrates that the forest floor acted as an annual net CO₂ source to the atmosphere at two contrasting boreal forest stands. We further found that the net forest floor CO₂ budget acted as the driving factor determining the variation of ecosystem-scale CO₂ balances across the two contrasting boreal forest stands within the same climatic region and at a similar stand developmental stage. This study therefore highlights the potential role of the forest floor in explaining the spatial variability of forest C budgets across mature forest stands in the boreal region. Our results also reveal that the net forest floor CO₂ source strength was enhanced during the summer drought year 2018 and the warmer non-growing season 2019. Thus, extending our efforts in acquiring comprehensive data on forest floor CO₂ fluxes will be critical for improving our understanding of the contributions from various ecosystem components to the forest carbon balance and for accurate predictions of the boreal biome-climate change feedbacks.

Declaration of Competing Interest

The authors declare that they have no known competing financial interests or personal relationships that could have appeared to influence the work reported in this paper.

Acknowledgments

The study was funded by the Knut and Alice Wallenberg Foundation (grant no. 2015.0047). The study sites Svartberget and Rosinedalsheden are part of the Swedish Infrastructure for Ecosystem Science (SITES). Svartberget is also part of the Swedish Integrated Carbon Observation System (ICOS-Sweden) research infrastructure. Financial support from

the Swedish Research Council and contributing research institutes to both SITES and ICOS-Sweden are acknowledged. The lead author J.C. gratefully acknowledges the financial support from the Kempe Foundation (grant no. SMK-1743). We would like to thank Per Marklund, Paul Smith, and Giuseppe De Simon from the Svartberget Field Research Station (SLU Unit for Field-based Forest Research) for technical and logistic support.

Appendix A

Supplementary materials

Supplementary material associated with this article can be found, in the online version, at doi:10.1016/j.agrformet.2021.108454.

References

- Allen, C.D., et al., 2010. A global overview of drought and heat-induced tree mortality reveals emerging climate change risks for forests. *For. Ecol. Manag.* 259 (4), 660–684. <https://doi.org/10.1016/j.foreco.2009.09.001>.
- Aubinet, M., et al., 2001. Long term carbon dioxide exchange above a mixed forest in the Belgian Ardennes. *Agric. For. Meteorol.* 108 (4), 293–315. [https://doi.org/10.1016/S0168-1923\(01\)00244-1](https://doi.org/10.1016/S0168-1923(01)00244-1).
- Aurela, M., Laurila, T., Tuovinen, J.-P., 2002. Annual CO₂ balance of a subarctic fen in northern Europe: Importance of the wintertime efflux. *J. Geophys. Res. Atmos.* 107 (D21) <https://doi.org/10.1029/2002jd002055>.
- Baldocchi, D.D., 2003. Assessing the eddy covariance technique for evaluating carbon dioxide exchange rates of ecosystems: past, present and future. *Global Change Biol.* 9 (4), 479–492. <https://doi.org/10.1046/j.1365-2486.2003.00629.x>.
- Baldocchi, D.D., Meyers, T.P., 1991. Trace gas exchange above the floor of a deciduous forest: 1. Evaporation and CO₂ efflux. *J. Geophys. Res. Atmos.* 96 (D4), 7271–7285. <https://doi.org/10.1029/91jd00269>.
- Barr, A.G., et al., 2004. Inter-annual variability in the leaf area index of a boreal aspen-hazelnut forest in relation to net ecosystem production. *Agric. For. Meteorol.* 126 (3), 237–255. <https://doi.org/10.1016/j.agrformet.2004.06.011>.
- Bastos, A., et al., 2020. Direct and seasonal legacy effects of the 2018 heat wave and drought on European ecosystem productivity. *Sci. Adv.* 6 (24), eaba2724. <https://doi.org/10.1126/sciadv.aba2724>.
- Bergeron, O., Margolis, H.A., Coursolle, C., 2009. Forest floor carbon exchange of a boreal black spruce forest in eastern North America. *Biogeosciences* 6 (9), 1849–1864. <https://doi.org/10.5194/bg-6-1849-2009>.
- Bhupinderpal Singh, et al., 2003. Tree root and soil heterotrophic respiration as revealed by girdling of boreal Scots pine forest: extending observations beyond the first year. *Plant Cell Environ.* 26 (8), 1287–1296. <https://doi.org/10.1046/j.1365-3040.2003.01053.x>.
- Black, T.A., et al., 1996. Annual cycles of water vapour and carbon dioxide fluxes in and above a boreal aspen forest. *Glob. Change Biol.* 2 (3), 219–229. <https://doi.org/10.1111/j.1365-2486.1996.tb00074.x>.
- Bonan, G.B., 2008. Forests and climate change: Forcings, feedbacks, and the climate benefits of forests. *Science* 320 (5882), 1444–1449. <https://doi.org/10.1126/science.1155121>.
- Brunet, Y., 2020. Turbulent flow in plant canopies: historical perspective and overview. *Bound. Layer Meteorol.* <https://doi.org/10.1007/s10546-020-00560-7>.
- Ciais, P., et al., 2005. Europe-wide reduction in primary productivity caused by the heat and drought in 2003. *Nature* 437 (7058), 529–533. <https://doi.org/10.1038/nature03972>.
- Commene, R., et al., 2017. Carbon dioxide sources from Alaska driven by increasing early winter respiration from Arctic tundra. *PNAS* 114 (21), 5361–5366. <https://doi.org/10.1073/pnas.1618567114>.
- Constantin, J., Grelle, A., Ibrom, A., Morgenstern, K., 1999. Flux partitioning between understory and overstorey in a boreal spruce/pine forest determined by the eddy covariance method. *Agric. For. Meteorol.* 98–9, 629–643. [https://doi.org/10.1016/S0168-1923\(99\)00129-X](https://doi.org/10.1016/S0168-1923(99)00129-X).
- Falk, M., Paw, U. K.T., Wharton, S., Schroeder, M., 2005. Is soil respiration a major contributor to the carbon budget within a Pacific Northwest old-growth forest? *Agric. For. Meteorol.* 135 (1), 269–283. <https://doi.org/10.1016/j.agrformet.2005.12.005>.
- Faticchi, S., Pappas, C., Zscheischler, J., Leuzinger, S., 2019. Modelling carbon sources and sinks in terrestrial vegetation. *New Phytol.* 221 (2), 652–668. <https://doi.org/10.1111/nph.15451>.
- Finnigan, J., 2000. Turbulence in plant canopies. *Annu. Rev. Fluid Mech.* 32 (1), 519–571. <https://doi.org/10.1146/annurev.fluid.32.1.519>.
- Fratini, G., Ibrom, A., Arriga, N., Burba, G., Papale, D., 2012. Relative humidity effects on water vapour fluxes measured with closed-path eddy-covariance systems with short sampling lines. *Agric. For. Meteorol.* 165, 53–63. <https://doi.org/10.1016/j.agrformet.2012.05.018>.

- Gash, J.H.C., Culf, A.D., 1996. Applying a linear detrend to eddy correlation data in realtime. *Bound. Layer Meteorol.* 79 (3), 301–306. <https://doi.org/10.1007/bf00119443>.
- Gaumont-Guay, D., et al., 2014. Eight years of forest-floor CO₂ exchange in a boreal black spruce forest: Spatial integration and long-term temporal trends. *Agric. For. Meteorol.* 184 (0), 25–35. <https://doi.org/10.1016/j.agrformet.2013.08.010>.
- Goulden, M.L., Crill, P.M., 1997. Automated measurements of CO₂ exchange at the moss surface of a black spruce forest. *Tree Physiol.* 17 (8–9), 537–542. <https://doi.org/10.1093/treephys/17.8-9.537>.
- Graf, A., et al., 2020. Altered energy partitioning across terrestrial ecosystems in the European drought year 2018. *Philos. Trans. R. Soc. B* 375 (1810), 20190524. <https://doi.org/10.1098/rstb.2019.0524>.
- Griffis, T.J., et al., 2004. Seasonal variation and partitioning of ecosystem respiration in a southern boreal aspen forest. *Agric. For. Meteorol.* 125 (3), 207–223. <https://doi.org/10.1016/j.agrformet.2004.04.006>.
- Hasselquist, N.J., Metcalfe, D.B., Högberg, P., 2012. Contrasting effects of low and high nitrogen additions on soil CO₂ flux components and ectomycorrhizal fungal sporocarp production in a boreal forest. *Glob. Change Biol.* 18 (12), 3596–3605. <https://doi.org/10.1111/gcb.12001>.
- Henttonen, H.M., Nojd, P., Mäkinen, H., 2017. Environment-induced growth changes in the Finnish forests during 1971–2010—An analysis based on National Forest Inventory. *For. Ecol. Manag.* 386, 22–36. <https://doi.org/10.1016/j.foreco.2016.11.044>.
- Högberg, P., et al., 2001. Large-scale forest girdling shows that current photosynthesis drives soil respiration. *Nature* 411 (6839), 789–792. <https://doi.org/10.1038/35081058>.
- Ibrom, A., Dellwik, E., Flyvbjerg, H., Jensen, N.O., Pilegaard, K., 2007. Strong low-pass filtering effects on water vapour flux measurements with closed-path eddy correlation systems. *Agric. For. Meteorol.* 147 (3–4), 140–156. <https://doi.org/10.1016/j.agrformet.2007.07.007>.
- Ikawa, H., et al., 2015. Understory CO₂, sensible heat, and latent heat fluxes in a black spruce forest in interior Alaska. *Agric. For. Meteorol.* 214–215, 80–90. <https://doi.org/10.1016/j.agrformet.2015.08.247>.
- Iivessniemi, H., et al., 2009. Long-term measurements of the carbon balance of a boreal Scots pine dominated forest ecosystem. *Boreal Environ. Res.* 14 (4), 731–753.
- Jaros, N., et al., 2008. Carbon dioxide and energy flux partitioning between the understory and the overstorey of a maritime pine forest during a year with reduced soil water availability. *Agric. For. Meteorol.* 148 (10), 1508–1523. <https://doi.org/10.1016/j.agrformet.2008.05.001>.
- Jocher, G., et al., 2018. Impact of canopy decoupling and subcanopy advection on the annual carbon balance of a boreal Scots pine forest as derived from eddy covariance. *J. Geophys. Res. Biogeosci.* 123 (2), 303–325. <https://doi.org/10.1002/2017jg003988>.
- Jocher, G., et al., 2017. Apparent winter CO₂ uptake by a boreal forest due to decoupling. *Agric. For. Meteorol.* 232, 23–34. <https://doi.org/10.1016/j.agrformet.2016.08.002>.
- Kaimal, J.C., Wyngaard, J.C., Izumi, Y., Coté, O.R., 1972. Spectral characteristics of surface-layer turbulence. *Q. J. R. Meteorol. Soc.* 98 (417), 563–589. <https://doi.org/10.1002/qj.49709841707>.
- Katul, G.G., Albertson, J.D., 1999. Modeling CO₂ sources, sinks, and fluxes within a forest canopy. *J. Geophys. Res. Atmos.* 104 (D6), 6081–6091. <https://doi.org/10.1029/1998jd200114>.
- Keenan, T.F., et al., 2019. Widespread inhibition of daytime ecosystem respiration. *Nat. Ecol. Evol.* 3 (3), 407–415. <https://doi.org/10.1038/s41559-019-0809-2>.
- Kelliher, F.M., et al., 1999. Carbon dioxide efflux density from the floor of a central Siberian pine forest. *Agric. For. Meteorol.* 94 (3), 217–232. [https://doi.org/10.1016/S0168-1923\(99\)00014-3](https://doi.org/10.1016/S0168-1923(99)00014-3).
- Kljun, N., et al., 2007. Response of net ecosystem productivity of three boreal forest stands to drought. *Ecosystems* 10, 1039–1055. <https://doi.org/10.1007/s10021-007-9088-x>.
- Klosterhalfen, A., et al., 2019. Source partitioning of H₂O and CO₂ fluxes based on high-frequency eddy covariance data: a comparison between study sites. *Biogeosciences* 16 (6), 1111–1132. <https://doi.org/10.5194/bg-16-1111-2019>.
- Kolari, P., et al., 2006. Forest floor vegetation plays an important role in photosynthetic production of boreal forests. *For. Ecol. Manag.* 221 (1), 241–248. <https://doi.org/10.1016/j.foreco.2005.10.021>.
- Kotani, A., et al., 2019. Impact of unusually wet permafrost soil on understory vegetation and CO₂ exchange in a larch forest in eastern Siberia. *Agric. For. Meteorol.* 265, 295–309. <https://doi.org/10.1016/j.agrformet.2018.11.025>.
- Kulmala, L., et al., 2008. H₂O and CO₂ fluxes at the floor of a boreal pine forest. *Tellus B: Chem. Phys. Meteorol.* 60 (2), 167–178. <https://doi.org/10.1111/j.1600-0889.2007.00327.x>.
- Kulmala, L., et al., 2019. Inter- and intra-annual dynamics of photosynthesis differ between forest floor vegetation and tree canopy in a subarctic Scots pine stand. *Agric. For. Meteorol.* 271, 1–11. <https://doi.org/10.1016/j.agrformet.2019.02.029>.
- Kulmala, L., et al., 2011. Photosynthetic production of ground vegetation in different-aged Scots pine (*Pinus sylvestris*) forests. *Can. J. For. Res.* 41 (10), 2020–2030. <https://doi.org/10.1139/x11-121>.
- Lasslop, G., et al., 2010. Separation of net ecosystem exchange into assimilation and respiration using a light response curve approach: critical issues and global evaluation. *Glob. Change Biol.* 16 (1), 187–208. <https://doi.org/10.1111/j.1365-2486.2009.02041.x>.
- Laudon, H., et al., 2011. Patterns and dynamics of dissolved organic carbon (DOC) in boreal streams: The role of processes, connectivity, and scaling. *Ecosystems* 14 (6), 880–893. <https://doi.org/10.1007/s10021-011-9452-8>.
- Laudon, H., et al., 2013. The Krycklan Catchment Study—a flagship infrastructure for hydrology, biogeochemistry, and climate research in the boreal landscape. *Water Resour. Res.* 49 (10), 7154–7158. <https://doi.org/10.1002/wrcr.20520>.
- Launiainen, S., et al., 2005. Eddy covariance measurements of CO₂ and sensible and latent heat fluxes during a full year in a boreal pine forest trunk-space. *Boreal Environ. Res.* 10 (6), 569–588.
- Lim, H., et al., 2015. Inter-annual variability of precipitation constrains the production response of boreal *Pinus sylvestris* to nitrogen fertilization. *For. Ecol. Manag.* 348, 31–45. <https://doi.org/10.1016/j.foreco.2015.03.029>.
- Lindroth, A., et al., 2018. Effects of low thinning on carbon dioxide fluxes in a mixed hemiboreal forest. *Agric. For. Meteorol.* 262, 59–70. <https://doi.org/10.1016/j.agrformet.2018.06.021>.
- Lindroth, A., et al., 2020. Effects of drought and meteorological forcing on carbon and water fluxes in Nordic forests during the dry summer of 2018. *Philos. Trans. R. Soc. B* 375 (1810), 20190516. <https://doi.org/10.1098/rstb.2019.0516>.
- Ma, Z.H., et al., 2012. Regional drought-induced reduction in the biomass carbon sink of Canada's boreal forests. *PNAS* 109 (7), 2423–2427. <https://doi.org/10.1073/pnas.1111576109>.
- Manzoni, S., Schimel, J.P., Porporato, A., 2012. Responses of soil microbial communities to water stress: results from a meta-analysis. *Ecology* 93 (4), 930–938. <https://doi.org/10.1890/11-0026.1>.
- Mauder, M. and Foken, T., 2004. Documentation and instruction manual of the eddy covariance software package TK2. 1–67.
- Misson, L., et al., 2007. Partitioning forest carbon fluxes with overstorey and understory eddy-covariance measurements: a synthesis based on FLUXNET data. *Agric. For. Meteorol.* 144 (1–2), 14–31. <https://doi.org/10.1016/j.agrformet.2007.01.006>.
- Moncrieff, J., Clement, R., Finnigan, J., Meyers, T., 2004. Averaging, detrending, and filtering of Eddy covariance time series. In: Lee, X., Massman, W.J., Law, B.E. (Eds.), *Handbook of Micrometeorology*. Springer, Netherlands.
- Moncrieff, J.B., et al., 1997. A system to measure surface fluxes of momentum, sensible heat, water vapour and carbon dioxide. *J. Hydrol.* 188–189, 589–611. [https://doi.org/10.1016/S0022-1694\(96\)03194-0](https://doi.org/10.1016/S0022-1694(96)03194-0).
- Moore, C.J., 1986. Frequency response corrections for eddy correlation systems. *Bound. Layer Meteorol.* 37 (1), 17–35. <https://doi.org/10.1007/BF00122754>.
- Morén, A.-S., Lindroth, A., 2000. CO₂ exchange at the floor of a boreal forest. *Agric. For. Meteorol.* 101 (1), 1–14. [https://doi.org/10.1016/S0168-1923\(99\)00160-4](https://doi.org/10.1016/S0168-1923(99)00160-4).
- Natali, S.M., et al., 2019. Large loss of CO₂ in winter observed across the northern permafrost region. *Nat. Clim. Change*. <https://doi.org/10.1038/s41558-019-0592-8>.
- Palmroth, S., et al., 2019. Nitrogen supply and other controls of carbon uptake of understory vegetation in a boreal *Picea abies* forest. *Agric. For. Meteorol.* 276–277, 107620. <https://doi.org/10.1016/j.agrformet.2019.107620>.
- Palmroth, S., et al., 2005. Contrasting responses to drought of forest floor CO₂ efflux in a Loblolly pine plantation and a nearby Oak-Hickory forest. *Glob. Change Biol.* 11 (3), 421–434. <https://doi.org/10.1111/j.1365-2486.2005.00915.x>.
- Pan, Y., et al., 2011. A large and persistent carbon sink in the world's forests. *Science* 333 (6045), 988–993. <https://doi.org/10.1126/science.1201609>.
- Paul-Limoges, E., Wolf, S., Eugster, W., Hörtnagl, L., Buchmann, N., 2017. Below-canopy contributions to ecosystem CO₂ fluxes in a temperate mixed forest in Switzerland. *Agric. For. Meteorol.* 247, 582–596. <https://doi.org/10.1016/j.agrformet.2017.08.011>.
- Paul-Limoges, E., et al., 2020. Partitioning evapotranspiration with concurrent eddy covariance measurements in a mixed forest. *Agric. For. Meteorol.* 280, 107786. <https://doi.org/10.1016/j.agrformet.2019.107786>.
- Peichl, M., Brodeur, J.J., Khomik, M., Arain, M.A., 2010. Biometric and eddy-covariance based estimates of carbon fluxes in an age-sequence of temperate pine forests. *Agric. For. Meteorol.* 150 (7–8), 952–965. <https://doi.org/10.1016/j.agrformet.2010.03.002>.
- Peters, W., Bastos, A., Ciais, P., Vermeulen, A., 2020. A historical, geographical and ecological perspective on the 2018 European summer drought. *Philos. Trans. R. Soc. B* 375 (1810), 20190505. <https://doi.org/10.1098/rstb.2019.0505>.
- Poggi, D., Porporato, A., Ridolfi, L., Albertson, J.D., Katul, G.G., 2004. The effect of vegetation density on canopy sub-layer turbulence. *Bound. Layer Meteorol.* 111 (3), 565–587. <https://doi.org/10.1023/B:BOUN.00000016576.05621.73>.
- Poudel, B.C., et al., 2011. Effects of climate change on biomass production and substitution in north-central Sweden. *Biomass Bioenergy* 35 (10), 4340–4355. <https://doi.org/10.1016/j.biombioe.2011.08.005>.
- Rebmann, C., et al., 2012. *Eddy Covariance: A Practical Guide to Measurement and Data Analysis*. Springer, London.
- Reichstein, M., et al., 2007. Reduction of ecosystem productivity and respiration during the European summer 2003 climate anomaly: a joint flux tower, remote sensing and modelling analysis. *Glob. Change Biol.* 13 (3), 634–651. <https://doi.org/10.1111/j.1365-2486.2006.01224.x>.
- Reichstein, M., et al., 2005. On the separation of net ecosystem exchange into assimilation and ecosystem respiration: Review and improved algorithm. *Glob. Change Biol.* 11 (9), 1424–1439. <https://doi.org/10.1111/j.1365-2486.2005.001002.x>.
- Richardson, A.D., Hollinger, D.Y., 2005. Statistical modeling of ecosystem respiration using eddy covariance data: Maximum likelihood parameter estimation, and Monte Carlo simulation of model and parameter uncertainty, applied to three simple models. *Agric. For. Meteorol.* 131 (3–4), 191–208. <https://doi.org/10.1016/j.agrformet.2005.05.008>.
- Richardson, A.D., Hollinger, D.Y., 2007. A method to estimate the additional uncertainty in gap-filled NEE resulting from long gaps in the CO₂ flux record. *Agric. For. Meteorol.* 147 (3–4), 199–208. <https://doi.org/10.1016/j.agrformet.2007.06.004>.

- Russell, E.S., et al., 2018. Effects of thinning a forest stand on sub-canopy turbulence. *Agric. For. Meteorol.* 248, 295–305. <https://doi.org/10.1016/j.agrformet.2017.10.019>.
- Ryhti, K., et al., 2021. Partitioning of forest floor CO₂ emissions reveals the belowground interactions between different plant groups in a Scots pine stand in southern Finland. *Agric. For. Meteorol.* 297, 108266 <https://doi.org/10.1016/j.agrformet.2020.108266>.
- Sabbatini, S., et al., 2018. Eddy covariance raw data processing for CO₂ and energy fluxes calculation at ICOS ecosystem stations. *Int. Agrophys.* 32, 495–515. <https://doi.org/10.1515/intag-2017-0043>.
- Shibistova, O., et al., 2002. Annual ecosystem respiration budget for a *Pinus sylvestris* stand in central Siberia. *Tellus B: Chem. Phys. Meteorol.* 54 (5), 568–589. <https://doi.org/10.1034/j.1600-0889.2002.01488.x>.
- Shorohova, E., Kapitsa, E., Vanha-Majamaa, I., 2008. Decomposition of stumps in a chronosequence after clear-felling vs. clear-felling with prescribed burning in a southern boreal forest in Finland. *For. Ecol. Manag.* 255 (10), 3606–3612. <https://doi.org/10.1016/j.foreco.2008.02.042>.
- Smith, S.W., 1997. *The Scientist and Engineer's Guide to Digital Signal Processing*. California Technical Publishing, San Diego, California.
- Stull, R.B., 1988. *An Introduction to Boundary Layer Meteorology*. Springer, The Netherlands.
- Swanson, R.V., Flanagan, L.B., 2001. Environmental regulation of carbon dioxide exchange at the forest floor in a boreal black spruce ecosystem. *Agric. For. Meteorol.* 108 (3), 165–181. [https://doi.org/10.1016/S0168-1923\(01\)00243-X](https://doi.org/10.1016/S0168-1923(01)00243-X).
- Tarvainen, L., et al., 2017. Photosynthetic refixation varies along the stem and reduces CO₂ efflux in mature boreal *Pinus sylvestris* trees. *Tree Physiol.* 38 (4), 558–569. <https://doi.org/10.1093/treephys/tpx130>.
- Tarvainen, L., et al., 2020. Limited vertical CO₂ transport in stems of mature boreal *Pinus sylvestris* trees. *Tree Physiol.* <https://doi.org/10.1093/treephys/tpaa113>.
- Teramoto, M., Liang, N., Zeng, J., Saigusa, N., Takahashi, Y., 2017. Long-term chamber measurements reveal strong impacts of soil temperature on seasonal and inter-annual variation in understory CO₂ fluxes in a Japanese larch (*Larix kaempferi* Sarg.) forest. *Agric. For. Meteorol.*, 247, 194–206. <https://doi.org/10.1016/j.agrformet.2017.07.024>.
- Teutschbein, C., Grabs, T., Karlsen, R.H., Laudon, H., Bishop, K., 2015. Hydrological response to changing climate conditions: Spatial streamflow variability in the boreal region. *Water Resour. Res.* 51 (12), 9425–9446. <https://doi.org/10.1002/2015WR017337>.
- Thomas, C., et al., 2008. Estimating daytime subcanopy respiration from conditional sampling methods applied to multi-scalar high frequency turbulence time series. *Agric. For. Meteorol.* 148 (8), 1210–1229. <https://doi.org/10.1016/j.agrformet.2008.03.002>.
- Thomas, C.K., Martin, J.G., Law, B.E., Davis, K., 2013. Toward biologically meaningful net carbon exchange estimates for tall, dense canopies: Multi-level eddy covariance observations and canopy coupling regimes in a mature Douglas-fir forest in Oregon. *Agric. For. Meteorol.* 173, 14–27. <https://doi.org/10.1016/j.agrformet.2013.01.001>.
- Vickers, D., Mahrt, L., 1997. Quality control and flux sampling problems for tower and aircraft data. *J. Atmos. Ocean. Technol.* 14 (3), 512–526. [https://doi.org/10.1175/1520-0426\(1997\)014<0512:qcasp>2.0.co;2](https://doi.org/10.1175/1520-0426(1997)014<0512:qcasp>2.0.co;2).
- Vickers, D., Thomas, C.K., 2014. Observations of the scale-dependent turbulence and evaluation of the flux–gradient relationship for sensible heat for a closed Douglas-fir canopy in very weak wind conditions. *Atmos. Chem. Phys.* 14 (18), 9665–9676. <https://doi.org/10.5194/acp-14-9665-2014>.
- Welp, L.R., Randerson, J.T., Liu, H.P., 2007. The sensitivity of carbon fluxes to spring warming and summer drought depends on plant functional type in boreal forest ecosystems. *Agric. For. Meteorol.* 147 (3), 172–185. <https://doi.org/10.1016/j.agrformet.2007.07.010>.
- Wharton, S., Schroeder, M., Paw, U, K.T., Falk, M., Bible, K., 2009. Turbulence considerations for comparing ecosystem exchange over old-growth and clear-cut stands for limited fetch and complex canopy flow conditions. *Agric. For. Meteorol.* 149 (9), 1477–1490. <https://doi.org/10.1016/j.agrformet.2009.04.002>.
- Widén, B., 2002. Seasonal variation in forest-floor CO₂ exchange in a Swedish coniferous forest. *Agric. For. Meteorol.* 111 (4), 283–297. [https://doi.org/10.1016/S0168-1923\(02\)00026-6](https://doi.org/10.1016/S0168-1923(02)00026-6).
- Wilczak, J.M., Oncley, S.P., Stage, S.A., 2001. Sonic anemometer tilt correction algorithms. *Bound. Layer Meteorol.* 99 (1), 127–150. <https://doi.org/10.1023/a:1018966204465>.
- Wutzler, T., et al., 2018. Basic and extensible post-processing of eddy covariance flux data with REdyProc. *Biogeosciences* 15 (16), 5015–5030. <https://doi.org/10.5194/bg-15-5015-2018>.